Mechanical Systems and Signal Processing 169 (2022) 108718

Contents lists available at ScienceDirect

Mechanical Systems and Signal Processing

journal homepage: www.elsevier.com/locate/ymssp

Autoregressive matrix factorization for imputation and forecasting of spatiotemporal structural monitoring time series

Peijie Zhang [a,1], Pu Ren [b,1], Yang Liu [c,*], Hao Sun [d,e]

[a] Department of Bridge Engineering, College of Highway, Chang'an University, Xi'an, Shann Xi 710064, China
[b] Department of Civil and Environmental Engineering, Northeastern University, Boston, MA 02115, USA
[c] Department of Mechanical and Industrial Engineering, Northeastern University, Boston, MA 02115, USA
[d] Gaoling School of Artificial Intelligence, Renmin University of China, Beijing, 100872, China
[e] Beijing Key Laboratory of Big Data Management and Analysis Methods, Beijing, 100872, China

ARTICLE INFO

Communicated by I. Kougioumtzoglou

Keywords:
Autoregressive
Matrix factorization
Data imputation
Time series forecasting
Spatiotemporal
Structural health monitoring

ABSTRACT

Reconstruction and prediction of spatiotemporal time series data has been a classic problem in structural health monitoring (SHM) in civil engineering applications. However, due to the explosive growth of sensing data, traditional time series analysis approaches fail in handling large-scale data with missing values. To this end, two autoregressive (AR) based matrix factorization (MF) methods are presented for missing sensor data imputation and structural response forecasting. The first model integrates the standard MF formulation with an innovative graph-based temporal regularizer, which can effectively model the nonlinear dynamics of SHM data and is computationally efficient, while the second approach introduces an additional AR-based matrix to better simulate the temporal factor thanks to its capability of learning the details of temporal evolution. Finally, the proposed methods are evaluated by using a field-recorded SHM dataset of a municipal concrete bridge, considering various missing scenarios (i.e., random, structured and mixed). The results demonstrate excellent performance of the methods which accurately recover missing entries in the time series and forecast future response. Additionally, the parametric analysis on model parameters indicates that reasonably higher rank and longer time lag improve the estimation accuracy while saving computational cost.

1. Introduction

In recent decades, the rapid development of sensor and wireless communication technologies facilitates the wide application of structural health monitoring (SHM) systems to various civil infrastructures, including momentous buildings and bridges. Typically, these systems receive and store the field-sensing data from structures and ambient environment through a series of functional modules that are comprised of sensory sector, data acquisition module, local centralized computer components and global central computer system. Not only does the collected data serve for the current structural performance evaluation, but also offers a platform for damage warning and reliable prediction of long-term serviceability. Nevertheless, there arises a challenge that high-quality data is usually required for these structural analysis tasks, meanwhile, the data anomalies (e.g., missing values and outliers) are inevitable in the monitoring period due to sensor malfunctions and power failure. These crucial issues have been attracting vast research interest in the field of data cleansing or preprocessing, and further response forecasting with imperfect data.

* Corresponding author.
E-mail addresses: yang1.liu@northeastern.edu (Y. Liu), haosun@ruc.edu.cn (H. Sun).
[1] Peijie Zhang and Pu Ren contribute equally to this work.

https://doi.org/10.1016/j.ymssp.2021.108718
Received 29 July 2021; Received in revised form 1 November 2021; Accepted 1 December 2021
Available online 7 January 2022

All of these tasks depend on the computational modeling and approximation of underlying structural dynamics. The traditional time series analysis methods mainly cover autoregressive (AR) models and dynamic linear models (DLM) [1,2], and are further extended to more intricate and feasible probabilistic models applied in the specific domains of SHM [3–9]. However, these classic approaches have fallen into the tough situation of computational inefficiency when processing large-scale datasets. For instance, considering a dataset collected from N sensors with T time stamps, the computational cost reaches $O(kN^2T + k^3T)$ by using the standard Kalman filter based DLM method, where k is the dimension of latent features and usually larger than N [10,11]. Herein, the multivariate time series problems become intractable due to considerable number of sensors and long-term monitoring period (i.e., large N and T) in real-world SHM. Additionally, Gaussian process (GP) also shows excellent capability in nonlinear structural response modeling [12–18], whereas still remains scalability issues and needs ideal prior assumptions. Moreover, especially in data reconstruction, compressive sensing (CS) [19–27] is extensively investigated thanks to its beautiful mathematical principle but the performance largely relies on the optimization approach and the sparsity of collected data. Specifically, based on the traditional CS principle, many algorithms have been proposed to improve the data recovery performance in the field of SHM, mainly covering Bayesian CS [20], adaptive wavelet based methods [23,24] and the spectro-temporal scheme [25]. It is also worthwhile to mention that the general idea of sparse representation has also been extended to structural damage identification [28]. Recently, the rapid advances in deep learning have lead to a proliferation of interesting studies in dynamical response prediction/modeling from both data-driven [29–31] and physics-informed [32–34] perspectives. In spite of the outstanding nonlinear fitting ability for surrogate modeling, they may encounter plights when dealing with missing values, and be short of generalization.

Hence, the challenging forecasting task based on large-scale datasets with missing values has been an inescapable obstacle in SHM. To this end, we seek to the resurgent matrix/tensor factorization (MF/TF) approaches [35–37] for solving such multi-dimensional time series problem in consideration of its natural strength in promoting high computational efficiency through decomposing the high-dimensional data into low-dimensional factors with low-rank assumption. The inspiration also comes from the empirical observation of the intrinsic correlation between structural dynamical responses, which well poses a low-rank and sparse-representation condition. MF/TF methods have already been widely adopted in biomedical science [36,38], wireless network engineering [37,39,40], traffic modeling [41–44], ranging from missing data imputation to pattern discovery, etc. In addition, there are also several attempts integrating the matrix/tensor factorization with current research interests in SHM. For instance, these methods are employed for data recovery [45], blind denoising [46], and computational cost reduction in finite element simulations [47]. However, the majority of previous matrix factorization (MF) methods capture latent temporal features directly based on the inner product of two factor matrices, which are incapable of predicting future time series data. To resolve this problem, graph-based approaches [48,49] and autoregressive (AR) process [11,50,51] are introduced into MF for explicitly modeling temporal propagation.

The main contribution of this paper is to investigate the refreshing theory of autoregressive matrix factorization for sensing data imputation and forecasting in SHM, and further propose a novel algorithm to improve the captured details of time series data. Firstly, we apply the temporal regularized matrix factorization (TRMF) method proposed by Yu et al. [11], which factorizes the imperfect sensor data matrix into spatial factor and temporal factor as well as innovates in the AR temporal regularizer. Secondly, we improve the classic AR-based MF method by introducing an additional matrix with AR process and further constructing the temporal factor matrix. In addition, we validate the performance of AR-based MF methods by using the SHM dataset recorded from a concrete bridge. The experimental results demonstrate that they can effectively capture the spatiotemporal evolution with satisfactory computational efficiency. We further implement the analysis on the model hyper-parameters which helps provide insights on the selection of rank and time lags.

The following sections of this paper is structured as follows: Section 2 describes the problem setup and introduces the theoretical background of two AR-based MF methods. The relationship between these two approaches and the comparison with classic time series analysis are also included. In Section 3, we test the AR-based MF methods with a temperature dataset under different missing scenarios. Besides, we also analyze the effects of model hyper-parameters. Section 4 concludes the entire paper.

2. Methodology

2.1. Problem statement

In this work we tackle the continuous SHM data imputation and forecasting problem by applying the MF scheme and leveraging the AR process on latent temporal factor. Herein, we consider the sensing data as a spatiotemporal matrix $\mathbf{Y} \in \mathbb{R}^{L\times T}$, which is collected from L sensor locations within T time stamps. Generally, given partially observed multidimensional time series, our goal is to estimate the historical missing values and provide a reliable prediction for the future response. In the context of MF, we can reach this target by learning the latent spatial factor $\mathbf{S} \in \mathbb{R}^{K\times L}$ and temporal factor $\mathbf{P} \in \mathbb{R}^{K\times T}$ which represent the inter-sensor effects and temporal propagation features respectively, where K is the rank of a specific matrix. As shown in Fig. 1, the mathematical formulation of MF is given by $\mathbf{Y} \approx \mathbf{S}^\top\mathbf{P}$.

In specific, at the sensor location i, we denote the imperfect time series as

$$\mathbf{Y}_i = (Y_{i,1}, Y_{i,2}, \dots, Y_{i,T}). \tag{1}$$

The imputation process aims to recover the unobserved data with the imputed values at corresponding time stamps, while the response forecasting for future τ time stamps (i.e., $(Y_{i,T+1}, \dots, Y_{i,T+\tau})$) relies on the dynamical AR process and the learned spatial factor and temporal factor.

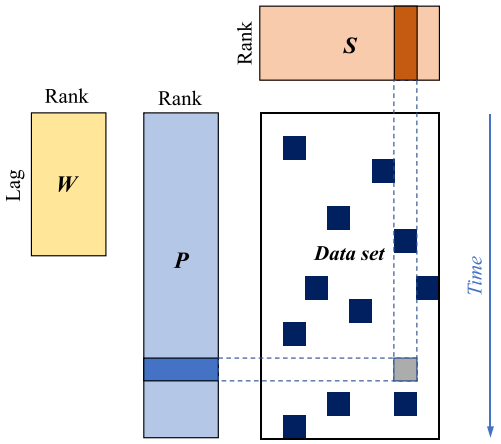

Fig. 1. Temporal regularized matrix factorization for SHM data with missing data.

2.2. Temporal regularized matrix factorization

Classic time series data analysis methods always suffer from the high computational cost when dealing with large-scale sensing data. To handle this, we investigate the application of temporal regularized matrix factorization (TRMF) [11], for explicitly modeling the temporal propagation on latent features based on the MF scheme. The basic components of MF are the spatial factor $\mathbf{S}$ (colored red) and the temporal factor $\mathbf{P}$ (colored blue) as shown in Fig. 1. The missing entries during the monitoring period are marked as dark squares. Element-wisely, the estimated signal $\widehat{Y}_{i,t}$ is given by

$$\widehat{Y}_{i,t} = \mathbf{S}_i^{\top}\mathbf{P}_t \tag{2}$$

where $\mathbf{S}_i^{\top}$ and $\mathbf{P}_t$ denotes the ith row vector of spatial factor and tth column vector of temporal matrix, respectively.

Furthermore, we adopt the graph-based regularization on the temporal factor which captures the dynamical dependencies between variables and holds better interpretability for time series data compared with the standard MF methods [11,52]. The $\mathbf{W}$ (colored yellow) in Fig. 1 plays the role of weighting factor in the time series analysis, which refers to the AR model in this paper. Thus, the estimated element can be further extended by

$$\widehat{Y}_{i,t} = \sum_{r=1}^{K} S_{i,r}\left(\sum_{l\in\mathcal{L}} w_{l,r}P_{r,t-l}\right) \tag{3}$$

where r denotes the rth element in corresponding column of factor matrices, and $\mathcal{L}$ represents the length of time lag in AR process.

In specific, regarding the temporal dependency in AR process, Fig. 2 illustrates the inter-relationship between different variables at different time stamps, which further constructs the regularization on temporal factor $\mathbf{P}$ in the objective function. Herein, w_{i-j} is the edge weight between the ith element and jth element. Thus, the graph-based temporal regularizer is formulated as

$$\mathcal{G}(\mathbf{P}\mid\mathbf{W},\gamma) = \frac{1}{2}\sum_{l\in\mathcal{L}}\sum_{t:t>l}\mathbf{w}_l^{\top}\left(\mathbf{P}_t-\mathbf{P}_{t-l}\right)^2 + \frac{\gamma}{2}\sum_{t=1}^{T}\|\mathbf{P}_t\|^2 \tag{4}$$

where the first regularizer term works for learning the correlation between tth row and $(t-l)$-th row of temporal factor, and the second term guarantees the convexity. Besides, it is also notable that edge weights are always positive values in consideration of ensuring the convexity of $\mathcal{G}(\mathbf{P}\mid\mathbf{W},\gamma)$. Here γ is a weighting coefficient, and $\|\cdot\|^2$ denotes the Frobenius norm. Afterwards, by applying the graph-based temporal regularizer, the holistic optimization goal is given by

$$\min_{\mathbf{S},\mathbf{P},\mathbf{W}\geq\mathbf{0}}\sum_{(i,t)\in\Omega}\left(Y_{i,t}-\mathbf{S}_i^{\top}\mathbf{P}_t\right)^2 + \lambda_s\sum_{i=1}^{L}\|\mathbf{S}_i\|^2 + \frac{\lambda_p}{2}\sum_{l\in\mathcal{L}}\sum_{t:t>l}\mathbf{w}_l^{\top}\left(\mathbf{P}_t-\mathbf{P}_{t-l}\right)^2 + \frac{\lambda_p\gamma}{2}\sum_{t=1}^{T}\|\mathbf{P}_t\|^2. \tag{5}$$

Here λ_s and λ_p are the weighting hyper-parameters for spatial factor and temporal factor, respectively. The squared Frobenius norm for spatial factor is a common choice of regularization to avoid overfitting. Besides, Ω represents an indicator set for the observed elements in $\mathbf{Y}$.

However, here comes a challenging issue that $\mathbf{W}$ tends to yield to all-zero solution when updating the parameters in Eq. (4). To alleviate it, Temporal Regularized Matrix Factorization (TRMF) [11] introduces a novel temporal regularizer to avert the aforementioned limitation. The improved temporal regularization is based on the popular time series model with the formulation as [11]

$$\mathbf{P}_t = \sum_{l\in\mathcal{L}}\mathbf{w}_l^{\top}\mathbf{P}_{t-l} + \boldsymbol{\epsilon}_t \tag{6}$$

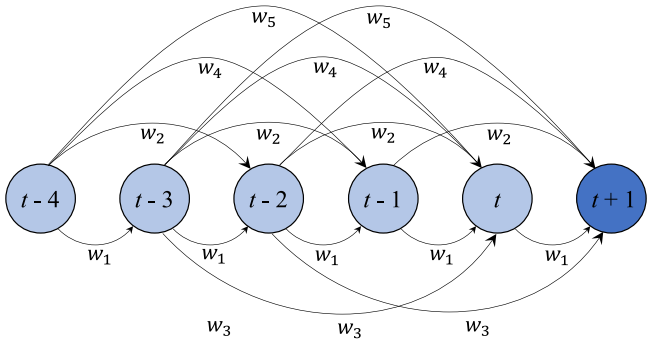

Fig. 2. An example of graph structure induced by the AR temporal regularizer with $\mathcal{L} = 1, 2, 3, 4$.

where l is in the lag set $\mathcal{L}$. Here ϵ_t is a zero mean Gaussian noise vector. Therefore, the new temporal regularizer [11] is realized by employing a negative log likelihood on the time series model: $-\log\mathbb{P}(\mathbf{P}_1, \ldots, \mathbf{P}_T \mid \mathbf{W})$. When the spatial factor $\mathbf{S}$ and the temporal feature matrix $\mathbf{P}$ are fixed, the optimization issue only lies in the weighting coefficients part,

$$\min_{\mathbf{W}} \mathcal{R}_{\mathrm{AR}}(\mathbf{P} \mid \mathbf{W}) + \lambda_w \mathcal{R}_w(\mathbf{W}) \tag{7}$$

where $\mathcal{R}_{\mathrm{AR}}(\mathbf{P} \mid \mathbf{W})$ denotes the regularizer for AR model and $\mathcal{R}_{\mathbf{W}}(\mathbf{W})$ represents the penalty on the parameters. Hence, it is reduced to a maximum-a-posterior (MAP) task for obtaining the optimal solution of $\mathbf{W}$. Thanks to this Bayesian setting, the notorious zero-solution issue can be prevented. Herein, the explicit formulation of the regularizer $\mathcal{R}_{\mathrm{AR}}$ in Eq. (7) are given by

$$\mathcal{R}_{\mathrm{AR}}\left(\overline{\mathbf{P}}_r \mid \mathcal{L}, \overline{\mathbf{w}}_r, \gamma\right) = \frac{1}{2} \sum_{t=1+M}^{T} \left(P_{r,t} - \sum_{l \in \mathcal{L}} w_{l,r} P_{r,t-l} \right)^2 + \frac{\gamma}{2} \|\overline{\mathbf{P}}_r\|^2, \tag{8}$$

where $\overline{\mathbf{w}}_r^\top$ and $\overline{\mathbf{P}}_r^\top$ are the rth rows of $\mathbf{W}$ and $\mathbf{P}$, respectively. Besides, M is an auxiliary parameter defined as $\max(\mathcal{L})$. Another characteristic establishment is to define the learned weighting matrix $\mathbf{W}$ as diagonal, which can improve the efficiency of training and still exhibit excellent performance for imputation and forecasting. Besides, the selection of lag set $\mathcal{L}$ is quite flexible. When dealing with long-range missing sensing data, we can set $\mathcal{L}$ to be large and even discontinuous to capture the dynamical and periodical patterns without huge computational efforts. Finally, the overall objective function is formulated as

$$\min_{\mathbf{S},\mathbf{P},\mathbf{W}} \sum_{(i,t)\in\Omega} \left(Y_{i,t} - \mathbf{S}_i^\top \mathbf{P}_t\right)^2 + \lambda_s \sum_{i=1}^{L} \|\mathbf{S}_i\|^2 + \sum_{r=1}^{K} \lambda_p \mathcal{R}_{\mathrm{AR}}\left(\overline{\mathbf{P}}_r \mid \mathcal{L}, \overline{\mathbf{w}}_r, \gamma\right) + \lambda_w \|\mathbf{W}\|^2, \tag{9}$$

which can be solved by using alternating minimization procedure. λ_w is the hyper-parameter for weighting matrix $\mathbf{W}$. First of all, we keep $\mathbf{P}$ and $\mathbf{W}$ fixed, and use alternating least square to update $\mathbf{S}$. Next, for updating $\mathbf{P}$, we utilize Graph Regularized Alternating Least Squares (GRALS) proposed in [53] to obtain the best estimation of

$$\arg\min_{\mathbf{P}} \sum_{(i,t)\in\Omega} \left(Y_{i,t} - \mathbf{S}_i^\top \mathbf{P}_t\right)^2 + \sum_{r=1}^{K} \lambda_p \mathcal{R}_{\mathrm{AR}}\left(\overline{\mathbf{P}}_r \mid \mathcal{L}, \overline{\mathbf{w}}_r, \gamma\right). \tag{10}$$

Lastly, with both $\mathbf{S}$ and $\mathbf{P}$ fixed, the optimization problem for updating $\mathbf{W}$ can be split into independent updating of each row of $\mathbf{W}$, which is given by

$$\arg\min_{\overline{\mathbf{w}}_r} \sum_{t=1+M}^{T} \left(P_{r,t} - \sum_{l \in \mathcal{L}} w_{l,r} P_{r,t-l} \right)^2 + \frac{\lambda_w}{\lambda_p} \|\overline{\mathbf{w}}_r\|^2. \tag{11}$$

The entire minimization can be seen as a ridge regression task solved with Cholesky factorization efficiently. For the selection of weighting coefficients, they are empirically determined via the grid search $\{\lambda_s, \lambda_p, \lambda_w\} \in \{0.5, 1, 2, 5, 10, 20, 50\}$. Herein, we set all of these three coefficients as 5 so that each loss component has the same scale in the optimization process.

2.3. AR-based matrix factorization

Next, the second AR-based MF method (i.e., ARMF) is proposed by designing a different temporal regularizer for learning dynamical evolution. Fig. 3 depicts the intrinsic philosophy of ARMF, where the right part mainly shows the MF scheme on the observed dataset and the left part presents the AR model respectively. We show the missing entries marked as dark squares in the right part of Fig. 3. First of all, for ARMF, the temporal factor matrix $\mathbf{P}$ (blue box) is formed as the product of the weight matrix $\mathbf{W}$ (yellow box) and the prepositive temporal factor matrix $\mathbf{Q}$ (both green part and light green part) considering AR process. Herein, different from TRMF, the AR-based part of ARMF has the form

$$\mathbf{P}_t = \sum_{l \in \mathcal{L}} \mathbf{w}_l^\top \mathbf{Q}_{t-l} + \epsilon_t. \tag{12}$$

Algorithm 1: Temporal Regularized Matrix Factorization (TRMF)

Input: the SHM data matrix $\mathbf{Y}$, the hyper-parameters λ_s, λ_p and λ_w, the iteration number N, the tensor rank K, the time lag $\mathcal{L}$ and the forecasting length τ.

Output: the approximation matrix $\widehat{\mathbf{Y}}_1$ and the predicted matrix $\widehat{\mathbf{Y}}_2$.

Initialize: random $\mathbf{P}$, $\mathbf{S}$ and $\mathbf{W}$;
$L, T = \mathbf{Y}.\texttt{size}$;
for $n = 1, \cdots, N$ **do**
  for $i = 1, \cdots, L$ **do**
    Update the spatial factor $\mathbf{S}_i$ (Eq. (9));
  end
  for $t = 1, \cdots, T$ **do**
    Fix the spatial matrix $\mathbf{S}$;
    Update the prepositive temporal factor $\mathbf{P}_t$ (Eq. (10));
  end
  for $l = 1, \cdots, \mathcal{L}$ **do**
    Fix the spatial and temporal matrices $\mathbf{S}$, $\mathbf{P}$;
    Update the weight matrix $\mathbf{W}_l$ (Eq. (11));
  end
end
// The imputation process
Compute $\widehat{Y}_1$ (Eq. (3));
// The forecasting process
for $j = 1, \cdots, \tau$ **do**
  Compute $\mathbf{P}_{T+j}$ (Eq. (6));
  Compute $\widehat{\mathbf{Y}}_2$ (Eq. (3));
end

Then the approximated spatiotemporal matrix $\widehat{\mathbf{Y}}$ is calculated by the inner product spatial factor $\mathbf{S}$ and temporal factor $\mathbf{P}$. Note that there is an additional part (light green box) attached in the beginning of the parallel temporal factor matrix, which can improve the imputation performance of the data in the beginning part. Herein, the basic principle of ARMF is to inherit the graph-based temporal regularizer and relieve the undesirable situation of zero-solution by utilizing the auxiliary matrix $\mathbf{Q}$. According to Eq. (12), we build the loss function as:

$$\min_{\mathbf{S},\mathbf{Q},\mathbf{W}} \sum_{(i,t)\in\Omega} \left(Y_{i,t} - \sum_{r=1}^{K} S_{i,r} \left(\sum_{l\in\mathcal{L}} w_{l,r} Q_{r,t-l} \right) \right)^2 + \lambda_q \|\mathbf{Q}\|^2 + \lambda_s \|\mathbf{S}\|^2 + \lambda_w \|\mathbf{W}\|^2 \tag{13}$$

where λ_q, λ_s and λ_w are the hyper-parameters for weighting different loss components. The regularizer on matrices $\mathbf{Q}$, $\mathbf{S}$ and $\mathbf{W}$ are designed for avoiding overfitting. The reason behind it lies in that the regularizers can constrain the parameter estimates towards zero and thus help the learned model escape from being too complex. The introduction of matrix $\mathbf{Q}$ promotes learning the correlation among the observed time series from multiple sensors, and prevents the issue of zero-solution.

We apply alternating minimization approach to get the best solution for this objective function in Eq. (13). The data imputation and forecasting tasks can be handled after the deriving these factor matrices $\mathbf{W}$, $\mathbf{Q}$ and $\mathbf{P}$. In specific, for updates $\mathbf{W}$, we aim to solve the sub-problem

$$\arg\min_{\mathbf{W}} \sum_{(i,t)\in\Omega} \left(Y_{i,t} - \sum_{r=1}^{K} \left(\sum_{l\in\mathcal{L}} w_{l,r} \cdot Q_{t+M-l,r} \right) S_{i,r} \right)^2 + \lambda_w \|\mathbf{W}\|^2, \tag{14}$$

when $\mathbf{Q}$ and $\mathbf{P}$ are fixed. Next, for updating $\mathbf{Q}$, the optimization problem is presented as

$$\arg\min_{\mathbf{Q}} \sum_{(i,t)\in\Omega} \left(Y_{i,t} - \sum_{r=1}^{K} \left(\sum_{l\in\mathcal{L}} w_{l,r} \cdot Q_{t+M-l,r} \right) S_{i,r} \right)^2 + \lambda_q \|\mathbf{Q}\|^2. \tag{15}$$

Finally, the updating for $\mathbf{S}$ equals to a simple matrix factorization problem as Eq. (2). The weighting coefficients are also determined with the grid search of $\{1, 10, 100, 200, 500, 800, 1000\}$. Here we select 500 for $\{\lambda_q, \lambda_s, \lambda_w\}$ in this paper.

2.4. Comparison between ARMF and TRMF

These two AR-based MF methods (i.e., TRMF and ARMF) share many similarities, but in the meanwhile, also hold their own characteristics. First of all, TRMF and ARMF both originate from the general MF scheme with the incorporation of AR process. Namely, they both largely rely on the temporal regularizer for modeling the dynamical responses. Nevertheless, the difference lies in the distinctive establishment of the temporal regularizer: (1) for TRMF, an innovative graph-based temporal regularizer is introduced to estimate the best solution of temporal factor matrix; (2) for ARMF, an auxiliary matrix $\mathbf{Q}$ is employed for improving

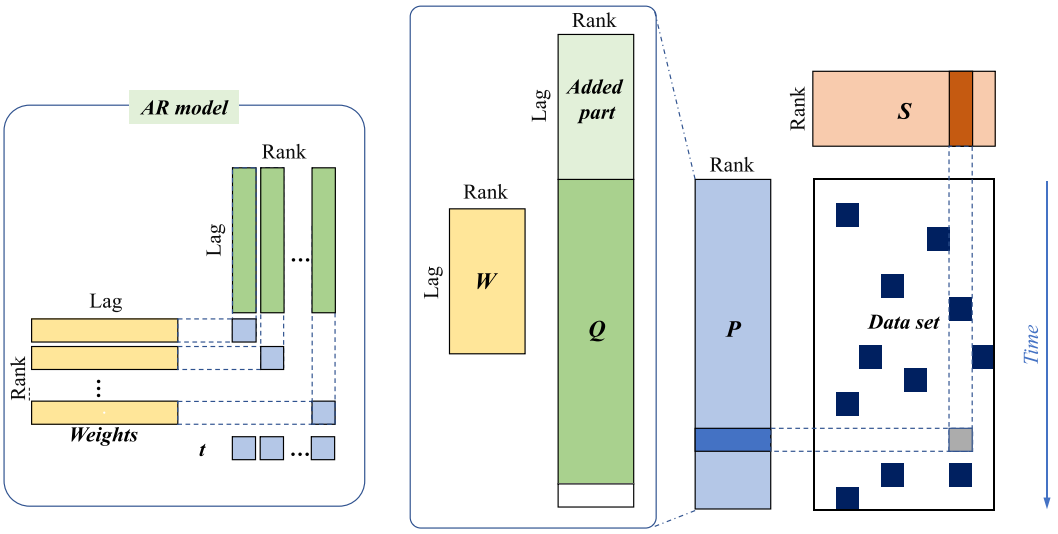

Fig. 3. Autoregressive-based matrix factorization for structural health monitoring data.

Algorithm 2: AR-based Matrix Factorization (ARMF)

Input: the SHM data matrix $\mathbf{Y}$, the hyper-parameters λ_q, λ_p and λ_w, the iteration number N, the tensor rank K, the time lag $\mathcal{L}$ and the forecasting length τ.

Output: the approximation matrix $\mathbf{A}_1$ and the predicted matrix $\mathbf{A}_2$.

Initialize: random $\mathbf{P}, \mathbf{Q}, \mathbf{S}, \mathbf{W}$;
$L, T = \mathbf{Y}.\texttt{size}$;
for $n = 1, \cdots, N$ **do**
  for $l = 1, \cdots, \mathcal{L}$ **do**
    Update the weight matrix $\mathbf{W}_l$ (Eq. (14));
  end
  for $t = 1, \cdots, T$ **do**
    Update the prepositive temporal factor $\mathbf{Q}_t$ (Eq. (15));
  end
  for $i = 1, \cdots, L$ **do**
    Compute the temporal factor matrix $\mathbf{P}$ (Eq. (12));
    Update the spatial factor $\mathbf{S}_i$ (Eq. (13));
  end
end
// The imputation process
Compute $\mathbf{A}_1 = \sum_{r=1}^{K} S_{i,r} \left(\sum_{l \in \mathcal{L}} w_{l,r} Q_{r,t-l} \right)$;
// The forecasting process
for $j = 1, \cdots, \tau$ **do**
  Compute $\mathbf{P}_{T+j}$ (Eq. (12));
  Compute $\mathbf{A}_2$;
end

the stability of temporal factor. The different strategies lead to varying performance based on theoretical and experimental analysis, mainly discussed in computational efficiency and estimation accuracy.

Computational efficiency. In each iteration, TRMF firstly conducts MF procedure to update $\mathbf{S}$, and then learns the temporal dependency of $\mathbf{P}$ and $\mathbf{W}$ using AR model. However, for ARMF, four factor matrices are updated based on all of the correlated observed entries directly, including the auxiliary matrix $\mathbf{Q}$. In specific, when updating weight matrix $\mathbf{W}$, ARMF applies the information of both current temporal factor matrix $\mathbf{P}$ and correlated observed entries, whereas TRMF only utilizes temporal factor matrix $\mathbf{P}$. Therefore, the convergence of TRMF is always faster than that of ARMF.

Accuracy. Theoretically, with the same setup of rank and time lags, TRMF and ARMF have very close performance for reconstruction/prediction after sufficient iterations. However, there is a slight difference between them. TRMF tends to show excellent performance for imputed/predicted results from a global perspective with averaged errors in multi-dimensional time series, whereas ARMF holds the strength in capturing the local details accurately (e.g., dramatic dynamics).

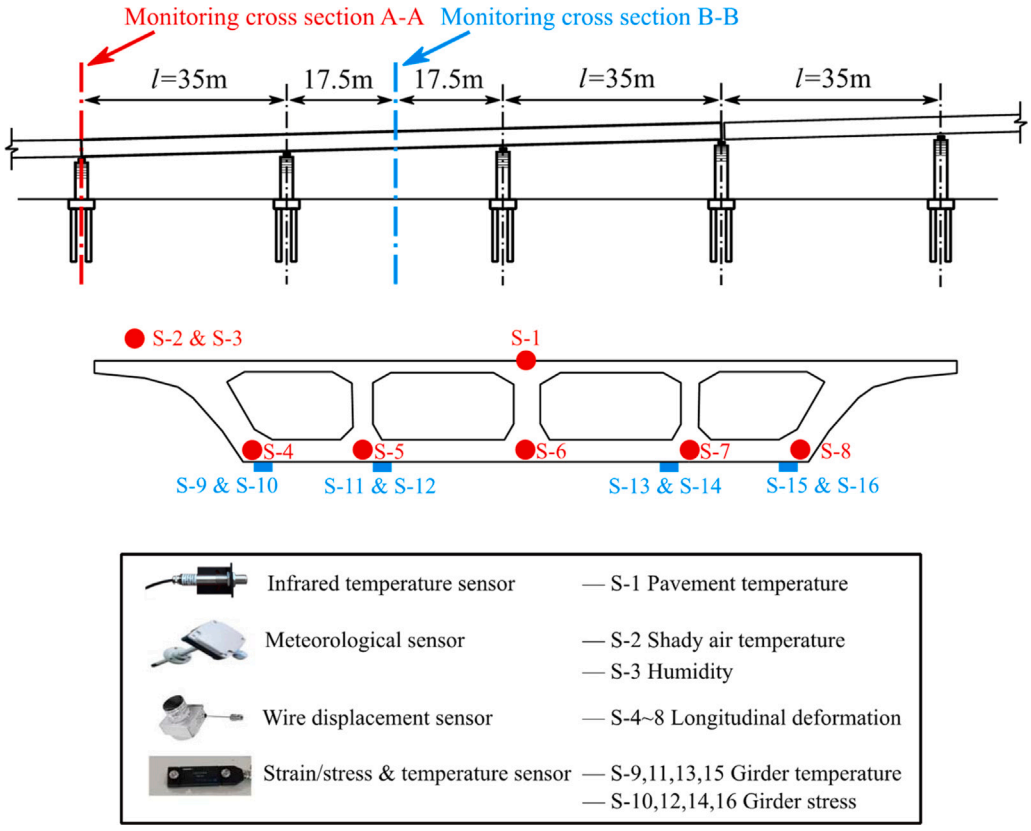

Fig. 4. Location and layout of sensors on the studied bridge

3. Experimental analysis

In this section, the imputation and forecasting performance of these two AR-based MF methods are evaluated through using the field-monitoring data recorded from a concrete box girder bridge. Distinctive and typical missing scenarios are simulated considering the real-world monitoring conditions. Furthermore, we dive deep into the sensitivity analysis of model parameters (i.e., rank and time lags) which essentially affect AR-based MF methods.

3.1. Field-tests description

The case bridge is a continuous concrete box girder bridge, comprised of 7 equal spans (i.e., 7 × 35 m). The depth of the girder is 2,000 mm, and the width of top plate and bottom plate are 26,000 mm and 17,000 mm respectively. As shown in Fig. 4, there are four types of sensing data collected from the investigated bridge, including temperature, humidity, displacement and stress. All these sensors were instrumented in the two cross sections (i.e., A–A and B–B). Specifically, the sensors located on the cross section A–A (at the pier), gather the environmental temperature, pavement temperature, humidity and longitudinal displacement. Moreover, we receive the stress and temperature information of the bottom plate from the cross section B–B (in the mid-span).

Herein, the dataset used for experimental validation contains 270-day SHM data collected from November 6, 2020 to August 3, 2021 with 1-hour interval (i.e., 24 time stamps in one day). Fig. 5 presents the dynamic patterns of the measurement data, where Figs. 5(a), 5(b), 5(c) and 5(d) showcase the time-series of temperature, humidity, displacement and stress, respectively. Considering the relevance across different types of sensing data and the correlation among the sensors of the same category, we utilize all of the measurements to conduct the experimental evaluation. In addition, we mainly investigate the imputation and forecasting performance on temperature, displacement and stress data as representative cases. Namely, we only set the missing scenarios on these three types of data, respectively.

3.2. Categories of missing data

Here we consider three missing scenarios simulated on the recorded SHM data: random missing, fiber missing and mixed missing. For the first scenario (random missing), the missing entries are randomly removed, which presents discrete and arbitrarily missing

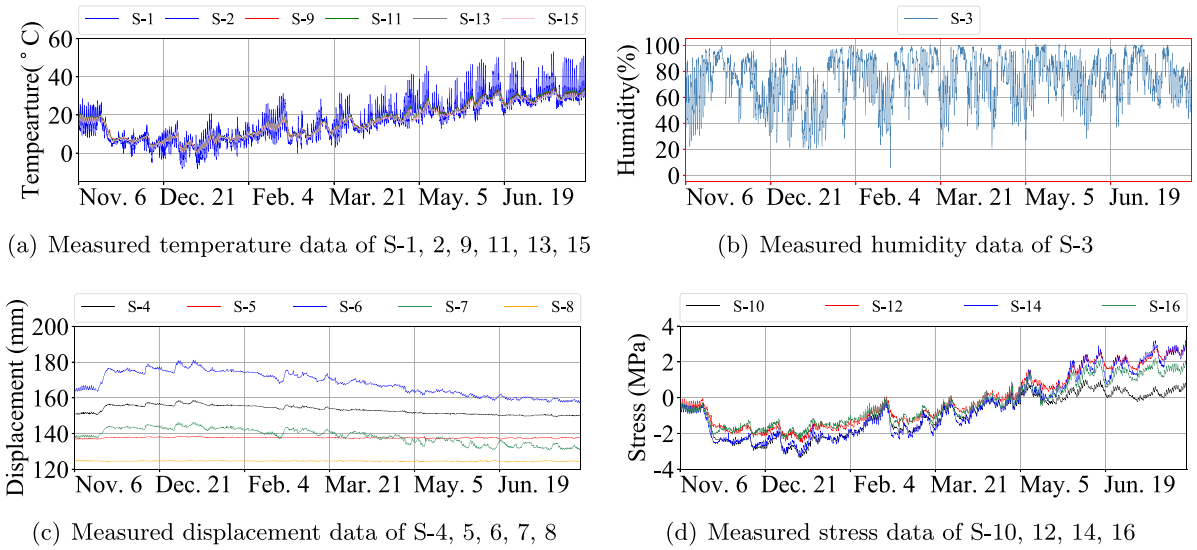

(a) Measured temperature data of S-1, 2, 9, 11, 13, 15

(b) Measured humidity data of S-3

(c) Measured displacement data of S-4, 5, 6, 7, 8

(d) Measured stress data of S-10, 12, 14, 16

Fig. 5. Time series of measured SHM data.

time histories. The random missing is usually induced by power fluctuation in the real-world monitoring. The second case (fiber missing) describes that missing data always show continuous corruptions over a period (e.g., one-day or several continuous days), which usually occurs due to sensors/system check, power off and software failure. To set the fiber missing experiments, we remove a certain proportion of continuous data with constant missing length h. Lastly, it is more common to simultaneously observe the random missing and the fiber missing appearing in the long-term monitoring period. Therefore, we define the mixed missing scenario which couples random missing and fiber missing and generates a more practical missing condition. The temperature data can be naturally organized as a matrix (16 sensors × 6480 time stamps).

In order to evaluate the imputation and forecasting performance of our proposed methods, we define a binary indicator matrix $\mathcal{I} \in \mathbb{R}^{L\times T}$ to record the missing positions, where 1 represents the observed entry while 0 marks the missing value. Therefore, given the fully-observed data matrix $\mathbf{Y}^*$, the sparse data matrix with missing entries $\mathbf{Y}$ is given by $\mathbf{Y}^* \odot \mathcal{I}$, where $\odot$ denotes the Hadamard product. Besides, we define an accuracy index to evaluate the effectiveness of AR-based MF methods, which is the root mean square error (RMSE) between the estimated results and the ground truth normalized by the root mean square of the target measurements. The formulation is given by

$$\rho = \left(1 - \frac{\sqrt{\frac{1}{n}\sum_{i=1}^{n}\left(\widehat{Y}_i - Y_i^*\right)^2}}{\sqrt{\frac{1}{n}\sum_{i=1}^{n}\left(Y_i^*\right)^2}}\right) \times 100\%. \tag{16}$$

Here $\widehat{Y}_i$ and Y_i^* are the reconstructed/predicted value and ground truth value at the corresponding position i respectively, where the measurement is missing or to be predicted. In addition, n is the total number of entries that need to be reconstructed/predicted.

3.3. Missing data imputation

As mentioned in Section 2, ARMF and TRMF share the similar graph structure of AR model, and the performance of them are close to each other when keeping same model parameters of the factor matrices. The testing results of imputation under random missing scenarios further demonstrate that these two methods have similar accuracy when missing rate is lower than 70%, as shown in Table 1. However, when the missing rate surpasses 70% (e.g., 80%), TRMF still performs robustly and reconstructs the missing measurements precisely, while ARMF shows inferior results. Hence, we apply TRMF to examine the imputation performance in different missing scenarios. Among all the experiments, the matrix rank is set as 8 and the maximum time lag is defined as 8.

For random missing scenarios, the sensor S-2 is selected as a typical example to present the imputation performance which is shown in Fig. 6. The overall missing rate η ranges from 20% to 80% with increment of 20%. We observe that the imputation results match well with ground truth, even when occurring large missing rate (i.e., over 50%). The excellent performance validates the effectiveness of AR-based matrix factorization methods, for capturing the nonlinear dynamics of time series data.

Secondly, for fiber missing, we define the missing rates covering from 10% to 50% increased by 10% for each scenario. Besides, we also investigate the influence of missing length h, which is defined as $h = \{1, 4, 7, 15\}$ days. As shown in Fig. 7, the imputation results of four different missing rates η with three missing length h demonstrate that AR-based MF approaches hold the remarkable

Table 1
Comparison of imputation accuracy between ARMF and TRMF under random missing scenarios.

Missing rate η [%]	Accuracy ρ [%]	
	TRMF	ARMF
10	99.70	99.50
20	99.59	99.33
30	99.36	98.83
40	98.95	98.55
50	98.93	98.08
60	98.71	96.21
70	97.87	93.39
80	90.47	80.72

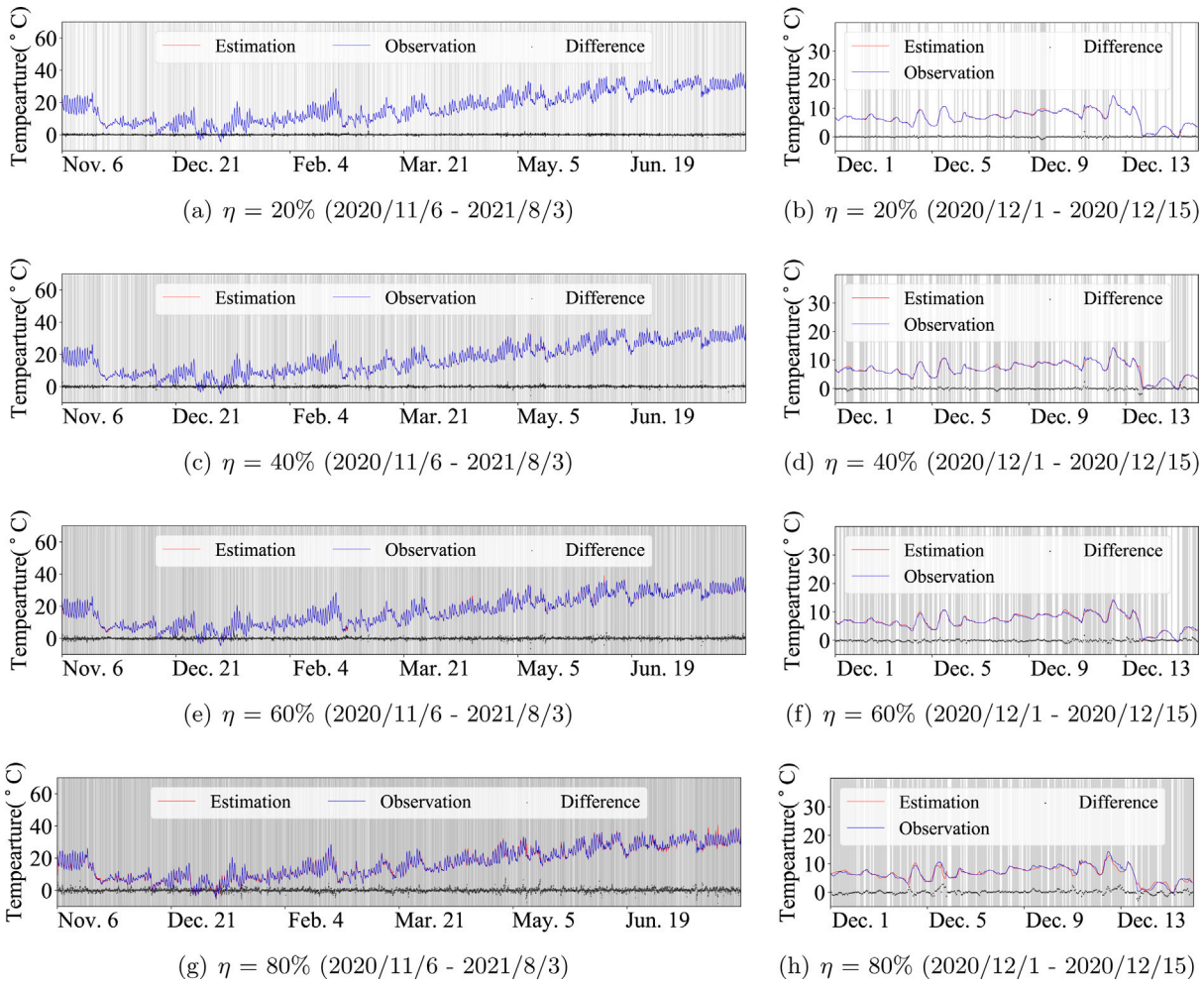

Fig. 6. The imputation results for four random missing cases of S-2. Note that the shading areas represent the time periods where data missing occurs, while the white areas denote that the strain time series are successfully recorded. Figs. 6(b), 6(d), 6(f), 6(h) are the zoom-in descriptions for four random missing scenarios.

capability for accurately modeling nonlinear time series data in general. The larger discrepancy can be observed in the extreme case (i.e., $\eta = 40\%$), especially with the larger missing length h.

Furthermore, we describe the details of the model performance and compare the accuracy of different missing scenarios with distinctive missing rates η and fiber missing length h, which are listed in Table 2. It is obvious that the overall trend is the estimation accuracy decreases when the missing rate η increases under the same missing rate condition, as well as when the missing length h enlarges with the same missing rate η. Nevertheless, there exist lower accuracy marked in bold in Table 2, which is caused by the data missing of all sensors occurs during the same time period. To figure out the effect of such harsh situation, we introduce a new

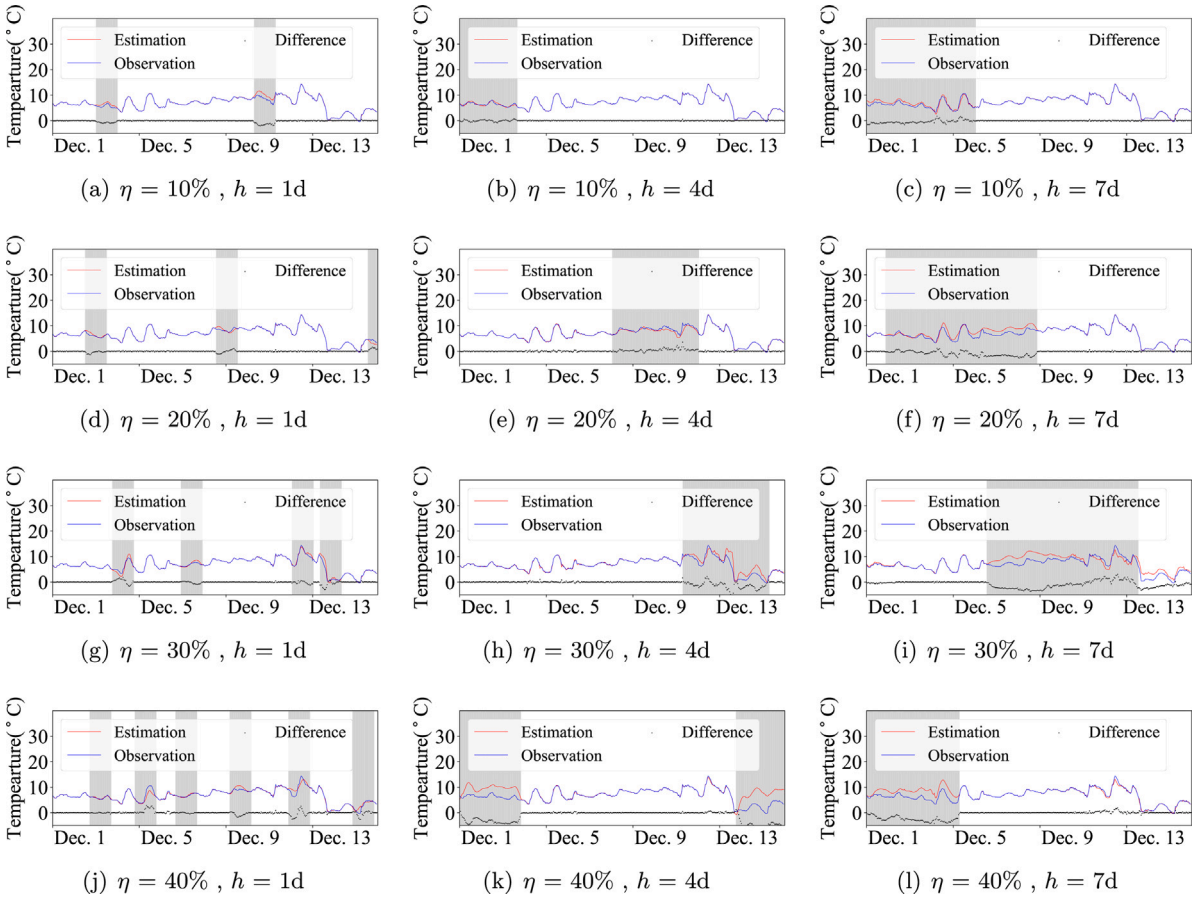

Fig. 7. The zoom-in imputation results for 12 fiber missing cases of S-2. Note that the shading areas represent the time periods where data missing occurs, while the white areas denote that the strain time series are successfully recorded. The symbol "d" denotes "days".

Table 2
Accuracy for different missing scenarios.

Missing rate η [%]	Accuracy ρ [%]			
	h = 1d	h = 4d	h = 7d	h = 15d
10	98.24	95.93	95.62	95.79
20	97.93	95.59	95.52	92.76
30	97.67	95.00	94.04	92.44
40	96.77	90.19	91.34	91.42
50	94.33	**78.64**	**69.16**	**63.04**

index κ to represent the proportion of data missing of all sensors in the same time. Herein, we test 100 random missing scenarios with the same overall missing rate ($\eta = 50\%$) but different κ by running TRMF method. The relationship between the index κ and the accuracy ρ is exhibited in Fig. 8, where the accuracy falls off with increasing κ.

In addition, while keeping all model parameters fixed, we further test two cases for mixed missing: (1) 30% fiber missing ($h = 4$d) combined with 20% random missing; (2) 20% fiber missing ($h = 4d$) mixed with 30% random missing. The representative imputation results of the sensor S-2 are shown in Fig. 9. Generally, the imputed data produces remarkable agreement with the ground truth. Moreover, the results in Case 2 own larger errors in data missing areas due to the larger κ of Case 2 compared with that of Case 1.

3.4. Forecasting with missing data

Thanks to the employment of AR process, we can easily predict the future structural response based on the observed time series data, even when the measurement data is imperfect. The dataset is split into two parts, where the first 75% segment is extracted for imputation and the rest 25% data is used for forecasting. Herein, we evaluate the prediction performance by testing the mixed missing scenario with 20% random missing and 10% fiber missing. The model parameters are same as those in Section 3.3

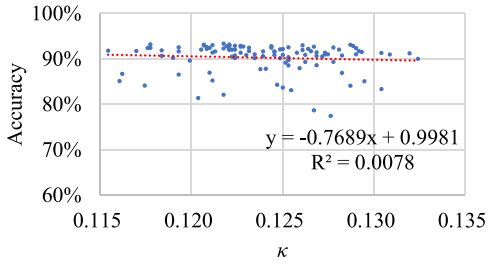

Fig. 8. Linear regression of accuracy and κ.

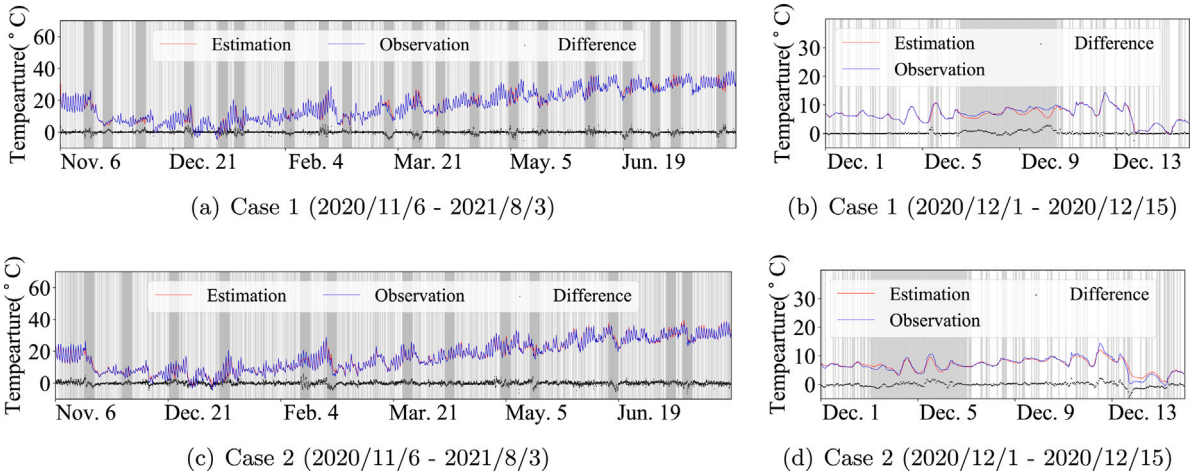

Fig. 9. The imputation results for two mixed missing cases of S-2. Note that the shading areas represent the time periods where data missing occurs, while the white areas denote that the temperature time series are successfully recorded.

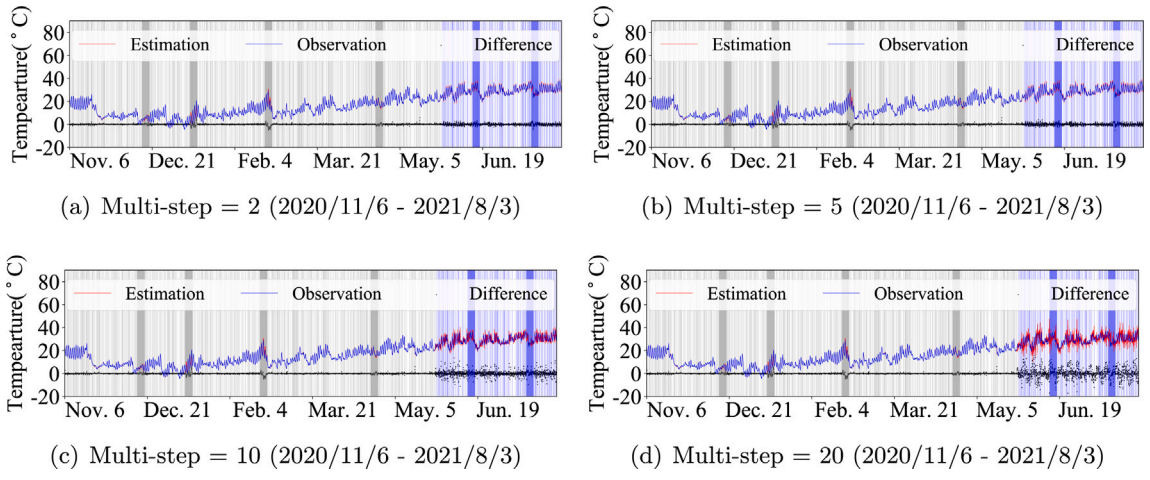

Fig. 10. The imputation and forecasting result for mixed missing at S-2. Note that the shading areas with dim-gray and light-blue represent the time periods where data missing occurs in observed period and predicted period respectively, while the white box areas denote that the temperature data are successfully recorded.

based on TRMF. In addition, we test 4 forecasting conditions with different steps (i.e., $\{2, 5, 10, 20\}$) in considering of the significant effect of the forward steps for prediction. The results are shown in Fig. 10. Both the imputed (i.e., before May. 26) and predicted (i.e., after May. 26) data well captures the overall dynamical patterns. Moreover, with the multi-step increasing, the difference between estimated results and the ground truth becomes larger but is still acceptable.

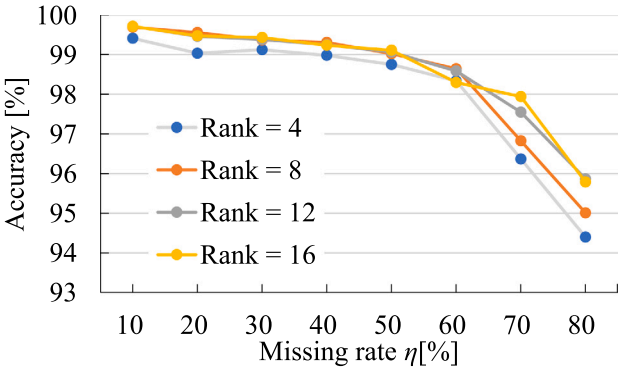

(a) Accuracy with different ranks

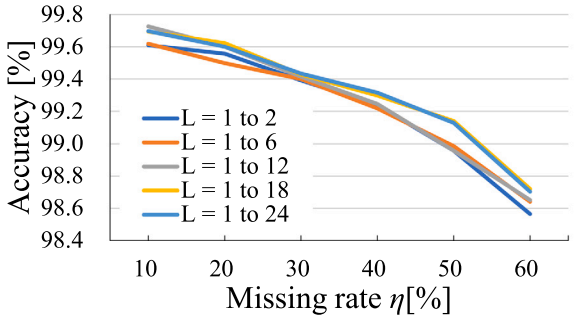

(b) Accuracy with different time lags

Fig. 11. The comparison of imputation performance with respect to different ranks and different lags.

3.5. Analysis of rank and time lags

Considering AR-based MF methods, the selection of rank and time lags is central to the performance of reconstruction/prediction. We implement the comparison experiments by using TRMF approach. Firstly, for rank analysis, we quantitatively investigate the performance of different ranks (i.e., $\{4, 8, 12, 16\}$) under different random missing scenarios with η ranging from 10% to 80%. As shown in Fig. 11(a), the overall trend is that higher ranks lead to higher accuracy when missing rate is less than 60%, but the accuracy improvement becomes mild and even worse with larger rank when η is larger than 60%. Obviously, there exists an optimal rank for the best imputation performance. Secondly, for time lags, we test and compare the performance by choosing 5 distinctive time lags under different random missing scenarios with η from 10% to 60%. The results are presented in Fig. 11(b). Generally, the models of longer time lags exhibit better imputation performance. Thus, the longer time lags can better capture the temporal dependencies due to more dynamical information learned and incorporated.

3.6. Extension to general SHM data

We also test on the displacement and stress data to evaluate the adaptation of AR-based MF methods to different types of monitoring data. Herein, we consider the 30% random missing scenario for testing the imputation performance. As shown in Fig. 12, our proposed approaches manifest the great match between the ground-truth observed data and the imputation values, which further validates their excellent capability of imputation for other types of SHM data as well. Therefore, the versatility is embraced by the AR-based MF methods, regardless of the magnitude or the variation of the measured data.

4. Conclusions

Inspired by the intrinsic low-rank structure in SHM data, this paper introduces two AR-based MF methods for sensing data imputation and prediction. These methods integrate the concept of AR process with MF scheme, which realize spatiotemporal learning and explicitly temporal dependency modeling simultaneously. In the experimental validation, we evaluate the performance of AR-based approaches under various missing scenarios, even the extremely large-scale missing conditions. The excellent reconstruction/prediction results demonstrate the effectiveness of AR-based MF methods with satisfactory computational efficiency. Besides, the significant analysis on model hyper-parameters provides the reasonable range for the selection of rank and time lags. In the

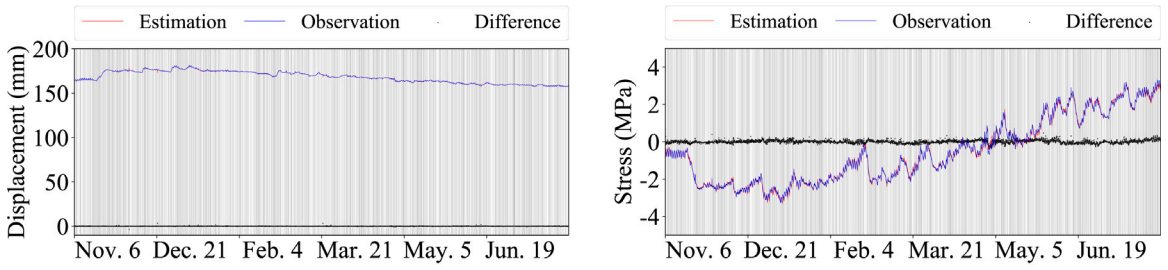

(a) Imputation results of displacement data (S-7) (b) Imputation results of stress data (S-15)

Fig. 12. The imputation results of other types of monitoring data.

future, based on the current investigation, we can further incorporate the physical laws into the AR-based MF model, which will make the learning process more robust and faster to converge.

CRediT authorship contribution statement

Peijie Zhang: Methodology, Software, Validation, Formal analysis, Investigation, Writing – original draft. **Pu Ren:** Methodology, Software, Validation, Formal analysis, Investigation, Writing – original draft. **Yang Liu:** Methodology, Writing – review & editing, Supervision. **Hao Sun:** Conceptualization, Methodology, Writing – review & editing, Supervision.

Declaration of competing interest

The authors declare that they have no known competing financial interests or personal relationships that could have appeared to influence the work reported in this paper.

Acknowledgment

The first author would like to thank the support from Chang'an University Short-Term Study Abroad Program for Postgraduate Students. The first author also acknowledges the support during his doctoral study from Dr. Chunsheng Wang. The last author would like to acknowledge the support in part by the Beijing Outstanding Young Scientist Program (No. BJJWZYJH012019100020098) as well as the Intelligent Social Governance Platform, Major Innovation & Planning Interdisciplinary Platform for the "Double-First Class" Initiative, Renmin University of China.

References

[1] R.E. Kalman, A new approach to linear filtering and prediction problems, 1960.
[2] M. West, J. Harrison, Bayesian Forecasting and Dynamic Models, Springer Science & Business Media, 2006.
[3] D. Lu, X. Fan, BayesIan forecasting of structural bending capacity of aging bridges based on dynamic linear model, in: Life-Cycle and Sustainability of Civil Infrastructure Systems: Proceedings of the Third International Symposium on Life-Cycle Civil Engineering (IALCCE'12), Vienna, Austria, October 3-6, 2012, CRC Press, 2012, p. 98.
[4] F. Xue-Ping, L. Da-gang, BayesIan prediction of structural bearing capacity of aging bridges based on dynamic linear model, J. Harbin Inst. Technol. 12 (2012).
[5] I.K. Solhjell, BayesIan forecasting and dynamic models applied to strain data from the göta river bridge, 2009.
[6] J.-A. Goulet, BayesIan dynamic linear models for structural health monitoring, Struct. Control Health Monit. 24 (12) (2017) e2035.
[7] L.H. Nguyen, J.-A. Goulet, Anomaly detection with the switching kalman filter for structural health monitoring, Struct. Control Health Monit. 25 (4) (2018) e2136.
[8] H. Wang, Y.-M. Zhang, J.-X. Mao, H.-P. Wan, T.-Y. Tao, Q.-X. Zhu, Modeling and forecasting of temperature-induced strain of a long-span bridge using an improved Bayesian dynamic linear model, Eng. Struct. 192 (2019) 220–232.
[9] Y. Wang, Y. Ni, BayesIan dynamic forecasting of structural strain response using structural health monitoring data, Struct. Control Health Monit. 27 (8) (2020) e2575.
[10] G. Petris, S. Petrone, P. Campagnoli, Dynamic linear models, in: Dynamic Linear Models with R, Springer, 2009, pp. 31–84.
[11] H.-F. Yu, N. Rao, I.S. Dhillon, Temporal regularized matrix factorization for high-dimensional time series prediction, in: Advances in Neural Information Processing Systems, 2016, pp. 847–855.
[12] C.K. Williams, C.E. Rasmussen, Gaussian Processes for Machine Learning, Vol. 2, (3) MIT Press, Cambridge, MA, 2006.
[13] T. Ozaki, A bridge between nonlinear time series models and nonlinear stochastic dynamical systems: A local linearization approach, Statist. Sinica (1992) 113–135.
[14] K. Worden, E. Cross, On switching response surface models, with applications to the structural health monitoring of bridges, Mech. Syst. Signal Process. 98 (2018) 139–156.
[15] H.-P. Wan, Y.-Q. Ni, BayesIan multi-task learning methodology for reconstruction of structural health monitoring data, Struct. Health Monit. 18 (4) (2019) 1282–1309.
[16] L.D. Avendaño-Valencia, E.N. Chatzi, Modelling long-term vibration monitoring data with Gaussian process time-series models, IFAC-PapersOnLine 52 (28) (2019) 26–31.

[17] S. Ahmed, A. Amer, C.A. Varela, F. Kopsaftopoulos, Data-driven state awareness for fly-by-feel aerial vehicles via adaptive time series and gaussian process regression models, in: International Conference on Dynamic Data Driven Application Systems, Springer, 2020, pp. 57–65.
[18] A. Amer, F. Kopsaftopoulos, Probabilistic damage quantification via the integration of non-parametric time-series and Gaussian process regression models, Struct. Health Monit. 2019 (2019).
[19] Y. Bao, H. Li, X. Sun, Y. Yu, J. Ou, Compressive sampling–based data loss recovery for wireless sensor networks used in civil structural health monitoring, Struct. Health Monit. 12 (1) (2013) 78–95.
[20] Y. Huang, J.L. Beck, S. Wu, H. Li, Robust Bayesian compressive sensing for signals in structural health monitoring, Comput.-Aided Civ. Infrastruct. Eng. 29 (3) (2014) 160–179.
[21] Y. Bao, Y. Yu, H. Li, X. Mao, W. Jiao, Z. Zou, J. Ou, Compressive sensing-based lost data recovery of fast-moving wireless sensing for structural health monitoring, Struct. Control Health Monit. 22 (3) (2015) 433–448.
[22] Y. Huang, J.L. Beck, S. Wu, H. Li, BayesIan compressive sensing for approximately sparse signals and application to structural health monitoring signals for data loss recovery, Probab. Eng. Mech. 46 (2016) 62–79.
[23] L. Comerford, H. Jensen, F. Mayorga, M. Beer, I. Kougioumtzoglou, Compressive sensing with an adaptive wavelet basis for structural system response and reliability analysis under missing data, Comput. Struct. 182 (2017) 26–40.
[24] I.A. Kougioumtzoglou, K.R. dos Santos, L. Comerford, Incomplete data based parameter identification of nonlinear and time-variant oscillators with fractional derivative elements, Mech. Syst. Signal Process. 94 (2017) 279–296.
[25] R. Klis, E.N. Chatzi, Vibration monitoring via spectro-temporal compressive sensing for wireless sensor networks, Struct. Infrastructure Eng. 13 (1) (2017) 195–209.
[26] Y. Bao, Z. Tang, H. Li, Compressive-sensing data reconstruction for structural health monitoring: A machine-learning approach, Struct. Health Monit. 19 (1) (2020) 293–304.
[27] I.A. Kougioumtzoglou, I. Petromichelakis, A.F. Psaros, Sparse representations and compressive sampling approaches in engineering mechanics: A review of theoretical concepts and diverse applications, Probab. Eng. Mech. 61 (2020) 103082.
[28] C. Zhang, Y. Xu, Comparative studies on damage identification with tikhonov regularization and sparse regularization, Struct. Control Health Monit. 23 (3) (2016) 560–579.
[29] R. Zhang, Z. Chen, S. Chen, J. Zheng, O. Büyüköztürk, H. Sun, Deep long short-term memory networks for nonlinear structural seismic response prediction, Comput. Struct. 220 (2019) 55–68.
[30] C. Mylonas, I. Abdallah, E. Chatzi, Deep unsupervised learning for condition monitoring and prediction of high dimensional data with application on windfarm scada data, in: Model Validation and Uncertainty Quantification, Vol. 3, Springer, 2020, pp. 189–196.
[31] R. Zhang, L. Meng, Z. Mao, H. Sun, Spatiotemporal deep learning for bridge response forecasting, J. Struct. Eng. 147 (6) (2021) 04021070.
[32] R. Zhang, Y. Liu, H. Sun, Physics-informed multi-LSTM networks for metamodeling of nonlinear structures, Comput. Methods Appl. Mech. Engrg. 369 (2020) 113226.
[33] R. Zhang, Y. Liu, H. Sun, Physics-guided convolutional neural network (PhyCNN) for data-driven seismic response modeling, Eng. Struct. 215 (2020) 110704.
[34] S.S. Eshkevari, M. Takáč, S.N. Pakzad, M. Jahani, Dynnet: Physics-based neural architecture design for nonlinear structural response modeling and prediction, Eng. Struct. 229 (2021) 111582.
[35] T.G. Kolda, B.W. Bader, Tensor decompositions and applications, SIAM Rev. 51 (3) (2009) 455–500.
[36] Z. Chen, A. Cichocki, Nonnegative matrix factorization with temporal smoothness and/or spatial decorrelation constraints, Lab. Adv. Brain Signal Process., RIKEN, Tech. Rep. 68 (2005).
[37] S. Rallapalli, L. Qiu, Y. Zhang, Y.-C. Chen, Exploiting temporal stability and low-rank structure for localization in mobile networks, in: Proceedings of the Sixteenth Annual International Conference on Mobile Computing and Networking, 2010, pp. 161–172.
[38] K. Devarajan, Nonnegative matrix factorization: an analytical and interpretive tool in computational biology, PLoS Comput. Biol. 4 (7) (2008) e1000029.
[39] N. Saeed, T.Y. Al-Naffouri, M.-S. Alouini, Outlier detection and optimal anchor placement for 3-D underwater optical wireless sensor network localization, IEEE Trans. Commun. 67 (1) (2018) 611–622.
[40] C. Dorffer, M. Puigt, G. Delmaire, G. Roussel, Blind mobile sensor calibration using an informed nonnegative matrix factorization with a relaxed rendezvous model, in: 2016 IEEE International Conference on Acoustics, Speech and Signal Processing (ICASSP), IEEE, 2016, pp. 2941–2945.
[41] P. Ahmadi, R. Kaviani, I. Gholampour, M. Tabandeh, Modeling traffic motion patterns via non-negative matrix factorization, in: 2015 IEEE International Conference on Signal and Image Processing Applications (ICSIPA), IEEE, 2015, pp. 214–219.
[42] G. Trigeorgis, K. Bousmalis, S. Zafeiriou, B.W. Schuller, A deep matrix factorization method for learning attribute representations, IEEE Trans. Pattern Anal. Mach. Intell. 39 (3) (2016) 417–429.
[43] L. Sun, K.W. Axhausen, Understanding urban mobility patterns with a probabilistic tensor factorization framework, Transp. Res. B 91 (2016) 511–524.
[44] X. Chen, Z. He, L. Sun, A Bayesian tensor decomposition approach for spatiotemporal traffic data imputation, Transp. Res. C 98 (2019) 73–84.
[45] Y. Yang, S. Nagarajaiah, Harnessing data structure for recovery of randomly missing structural vibration responses time history: Sparse representation versus low-rank structure, Mech. Syst. Signal Process. 74 (2016) 165–182.
[46] Y. Yang, S. Nagarajaiah, Blind denoising of structural vibration responses with outliers via principal component pursuit, Struct. Control Health Monit. 21 (6) (2014) 962–978.
[47] M. Hariri-Ardebili, F. Pourkamali-Anaraki, Matrix completion for cost reduction in finite element simulations under hybrid uncertainties, Appl. Math. Model. 69 (2019) 164–180.
[48] M. Roughan, Y. Zhang, W. Willinger, L. Qiu, Spatio-temporal compressive sensing and internet traffic matrices (extended version), IEEE/ACM Trans. Netw. 20 (3) (2011) 662–676.
[49] L. Xiong, X. Chen, T.-K. Huang, J. Schneider, J.G. Carbonell, Temporal collaborative filtering with bayesian probabilistic tensor factorization, in: Proceedings of the 2010 SIAM International Conference on Data Mining, SIAM, 2010, pp. 211–222.
[50] X. Chen, L. Sun, BayesIan temporal factorization for multidimensional time series prediction, IEEE Trans. Pattern Anal. Mach. Intell. (2021).
[51] P. Ren, X. Chen, L. Sun, H. Sun, Incremental Bayesian matrix/tensor learning for structural monitoring data imputation and response forecasting, Mech. Syst. Signal Process. 158 (2021) 107734.
[52] E.J. Candès, X. Li, Y. Ma, J. Wright, Robust principal component analysis? J. ACM 58 (3) (2011) 1–37.
[53] N. Rao, H.-F. Yu, P. Ravikumar, I.S. Dhillon, Collaborative filtering with graph information: Consistency and scalable methods., in: NIPS, Vol. 2, (4) Citeseer, 2015, p. 7.